LETTERS
PUBLISHED ONLINE: 22 MARCH 2009 | DOI: 10.1038/NPHYS1217

nature physics

Tightly trapped acoustic phonons in photonic crystal fibres as highly nonlinear artificial Raman oscillators

M. S. Kang, A. Nazarkin, A. Brenn and P. St. J. Russell*

Interactions between light and hypersonic waves can be enhanced by tight field confinement, as shown in periodically structured materials[1], microcavities[2], micromechanical resonators[3] and photonic crystal fibres[4–6] (PCFs). There are many examples of weak sound–light interactions, for example, guided acoustic-wave Brillouin scattering in conventional optical fibres[7]. This forward-scattering effect results from the interaction of core-guided light with acoustic resonances of the entire fibre cross-section, and is viewed as a noise source in quantum-optics experiments[8]. Here, we report the observation of strongly nonlinear forward scattering of laser light by gigahertz acoustic vibrations, tightly trapped together in the small core of a silica–air PCF. Bouncing to and fro across the core at close to 90° to the fibre axis, the acoustic waves form optical-phonon-like modes with a flat dispersion curve and a distinct cutoff frequency Ω_a. This ensures automatic phase-matching to the guided optical mode so that, on pumping with a dual-frequency laser source tuned to Ω_a, multiple optical side bands are generated, spaced by Ω_a. The number of strong side bands in this Raman-like process increases with pump power. The results point to a new class of designable nonlinear optical device with applications in, for example, pulse synthesis, frequency comb generation for telecommunications and fibre laser mode-locking.

Confining light within a small volume leads to high electromagnetic field intensities and the enhancement of all kinds of nonlinear optical effect. Recent examples include the use of plasmon polaritons on metallic surfaces for high harmonic generation[9], nonlinear optical detection of proteins using gold colloids[10], proposals for single-photon transistors using plasmonic effects[11] and the use of high-Q microcavities for ultralow-threshold Raman lasers[12] and optical frequency comb generation[13].

Here, we show that phonon–photon interactions can also be strongly enhanced—by tight confinement of both sound and light in the core of a photonic crystal fibre (PCF). The vibrating core may be viewed as an artificial Raman oscillator of which the frequency, lifetime and optical overlap are designable by adjusting the core nanostructure. The mechanism of spectral broadening thus has similarities with that studied in Raman-active gases[14], although the use of tightly trapped acoustic vibrations as a highly nonlinear Raman oscillator has, to our knowledge, not previously been reported. Remarkably close agreement is obtained between the experimental results and the predictions of theory, indicating that all components in the frequency comb are mutually coherent, simultaneously creating and annihilating acoustic phonons through electrostrictive and stress-optical effects.

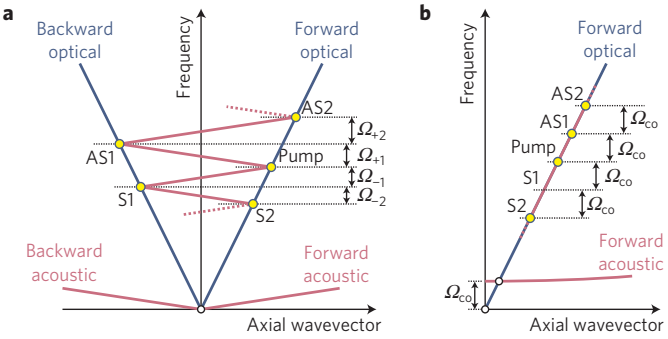

Figure 1 | Dispersion diagrams for guided optical and acoustic modes. The principles of backward Brillouin scattering and forward Raman-like scattering by acoustic phonons are illustrated (not to scale). For simplicity, the optical phase velocity is assumed independent of frequency. Positive/negative slopes indicate forward/backward phase velocities. **a**, In backward Brillouin scattering (acoustic phase velocity assumed constant), the frequency shift of each Stokes (S) and anti-Stokes (AS) order is different, and the phonon direction alternates between successive orders. **b**, In forward Raman-like scattering, the acoustic dispersion is nonlinear, exhibiting a cutoff frequency Ω_{co}; this means that phase-matching between successive Stokes and anti-Stokes orders is automatic, the frequency-spacing between them remaining constant.

The effect differs markedly from stimulated Brillouin scattering (SBS) in optical fibres, where fibre lengths of several hundred metres and a few milliwatts of laser power are sufficient to observe efficient generation of a backward-propagating frequency-down-shifted Stokes wave[15–17]. The generation of multiple side bands by SBS is difficult, however, because the Brillouin frequency shifts required for phase-matching are proportional to the laser pump frequency, and furthermore the phonon direction alternates between successive side bands (Fig. 1a). These factors, together with the backward nature of the interaction, render cascaded SBS interactions very inefficient, requiring strong feedback[18,19]. In strong contrast, Raman-like scattering from transversely trapped acoustic phonons has a Stokes frequency shift that is independent of the laser pump frequency. Furthermore, the collinear and phase-matched character of the multi-wave parametric interaction enables the simultaneous accumulation of nonlinear response at all generated Stokes and anti-Stokes frequencies (Fig. 1b).

The silica–air PCF used in the experiments has a solid glass core (diameter 1.8 μm) surrounded by a hexagonal array of approximately circular hollow channels (diameter ~1.6 μm,

Max-Planck Institute for the Science of Light, Guenther-Scharowsky-Str. 1/Bau 24, 91058 Erlangen, Germany. *e-mail: philip.russell@mpl.mpg.de.

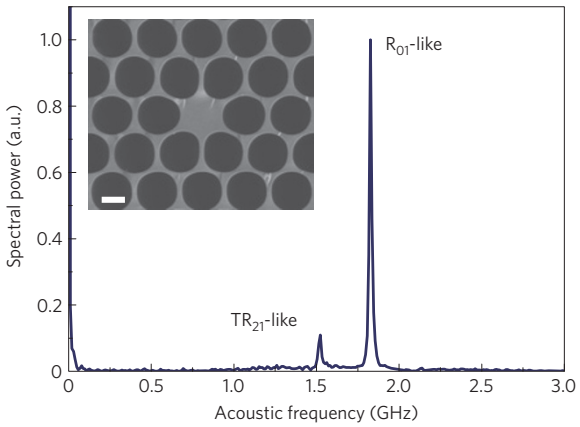

Figure 2 | Spectrum of acoustic resonances in the PCF used in the experiment. The inset is the scanning electron micrograph of the fibre cross-section, where the white horizontal bar corresponds to 1 μm. In the spectrum, the large peak at 1.83 GHz reveals acoustic phonons in the axially symmetric (breathing) R_{01}-like acoustic mode. The small peak at 1.52 GHz comes from acoustic phonons in the axially asymmetric TR_{21}-like acoustic mode. Both of them are acoustic modes confined in the core of the PCF.

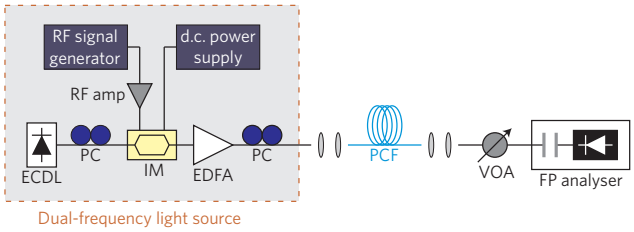

Figure 3 | Schematic diagram of the experimental set-up. A frequency-spacing-tunable dual-frequency light source is launched into the PCF. The optical spectrum of the transmitted light is measured with a Fabry–Perot (FP) spectrum analyser. ECDL, external cavity diode laser; PC, polarization controller; IM, intensity modulator; EDFA, erbium-doped fibre amplifier; VOA, variable optical attenuator.

air-filling fraction 74%—see the inset of Fig. 2). Confinement of acoustic phonons results from the large impedance mismatch between air and glass, aided in certain cases by the appearance of phononic bandgaps.

The acoustic response of a 10 m length of PCF was first investigated by launching 100 ps laser pulses and monitoring the ensuing vibrations optically in a Sagnac loop (see Supplementary Section S1). Figure 2 shows a typical spectrum, with two acoustic resonances, each related to a different type of trapped acoustic phonon. The dominant peak at 1.83 GHz is caused by excitation of the R_{01}-like radial acoustic mode, whereas the weaker one at 1.52 GHz comes from the TR_{21}-like torsional–radial mode. The frequencies agree well with both theoretical calculations and measurements made previously using a different method[6]. We now focus attention on the R_{01}-like mode, because this is more efficiently excited, through electrostriction, by the fundamental optical guided mode[20].

Figure 3 shows the experimental set-up. An electro-optic modulator was used to synthesize a dual-frequency pump source from a single-frequency 1,550 nm external cavity diode laser. With a sinusoidal drive signal and appropriate d.c. bias[15], two equal amplitude side bands were generated, spaced by twice the frequency of the drive signal, while the central laser frequency was strongly suppressed. This dual-frequency signal was then amplified in an Er-doped fibre amplifier, and launched into the PCF. The optical spectrum of pump and transmitted light was measured using a Fabry–Perot spectrum analyser with free spectral range (FSR) 4 GHz and finesse 4,000 (Fig. 4).

The beat-note of the dual-frequency source was tuned to 1.83 GHz, so as to excite the R_{01}-like resonance, and a total optical power of 64 mW was launched into the PCF. Conversion to the lower-frequency (Stokes) band is clearly seen (Fig. 4b), roughly half the power at the higher frequency (at 0.9135 GHz) being transferred to the lower band (at -0.9135 GHz). Note that the optical spectrum is folded owing to the 4 GHz FSR of the Fabry–Perot spectrum analyser; as a result, the next-order Stokes and anti-Stokes components (actual relative frequencies $\mp$2.7405 GHz) appear at $\pm$1.26 GHz. Next, the dependence of the conversion on detuning of the dual-frequency pump was explored (Fig. 4c), showing pronounced resonant behaviour, with a bandwidth of 15 MHz (yielding a Q-factor of 1.83 GHz/15 MHz ~ 122). At resonance, the energy transferred increases monotonically with pump power (Fig. 4d). After fitting these measurements to theory (described below), the gain coefficient at line-centre is estimated to be 1.5 m^{-1} W^{-1}, implying that optical power levels of the order of tens of milliwatts are sufficient to observe stimulated Raman-like scattering in a 10 m length of PCF.

The linewidth Γ_B is inversely related to the lifetime of the acoustic resonance in the core (see below and Supplementary Section S2), which is expected to contain contributions from bulk viscosity, radiative leakage into the cladding, dissipation in the air and structural non-uniformities along the PCF length:

$$\Gamma_B = \frac{1}{\tau_{viscosity}} + \frac{1}{\tau_{leakage}} + \frac{1}{\tau_{air}} + \frac{1}{\tau_{inhomo}} \quad (1)$$

An estimate based on bulk viscosity in a vacuum-clad silica strand yields $1/\tau_{viscosity} \approx 750$ kHz, which is some 20 times smaller than the linewidth measured (15 MHz). It is likely that homogeneous (the first three terms) and inhomogeneous broadening both have a role, although leakage is likely to dominate in the PCF. The contribution from the air is likely to be very small, because of the huge discontinuity in the acoustic impedance between glass and air.

The electrostrictive force driving the transverse acoustic resonances is proportional to the gradient of the transverse intensity profile of the guided optical field[20,21]. The intensity pattern produced by the two co-propagating optical fields varies much faster along the transverse direction (across the small PCF core) than along the axial direction (the longitudinal period, or acoustic wavelength, is ~10 cm in our case). These considerations lead to analytical equations describing the Stokes process (see Supplementary Section S2):

$$\frac{\partial P_1}{\partial z} = gP_1P_2, \qquad \frac{\partial P_2}{\partial z} = -gP_1P_2$$

$$g(\Omega) = g_0 \frac{(\Gamma_B/2)^2}{(\Omega - \Omega_a)^2 + (\Gamma_B/2)^2} \quad (2)$$

$$g_0 = \frac{\omega_1 \gamma_e^2 |Q_0 Q_1|}{2n_{eff}^2 c^2 \rho_0 \Omega_a \Gamma_B}$$

where P_1 and P_2 are the optical powers of the Stokes and the pump wave, respectively, $g(\Omega)$ represents the gain spectrum and g_0 is the gain coefficient at resonance. In addition, γ_e is the electrostrictive constant, n_{eff} is the axial refractive index of the optical mode in the PCF, c is the velocity of light in vacuum and ρ_0 is the mean density of silica. Q_0 and Q_1 are defined as $Q_0 \equiv \langle E_0^2, \rho_{01} \rangle$ and $Q_1 \equiv \langle \nabla_\perp (E_0^2), \rho_{01} \rangle$, where $E_0(r)$ is the field distribution of the optical mode and $\rho_{01}(r)$ is the density

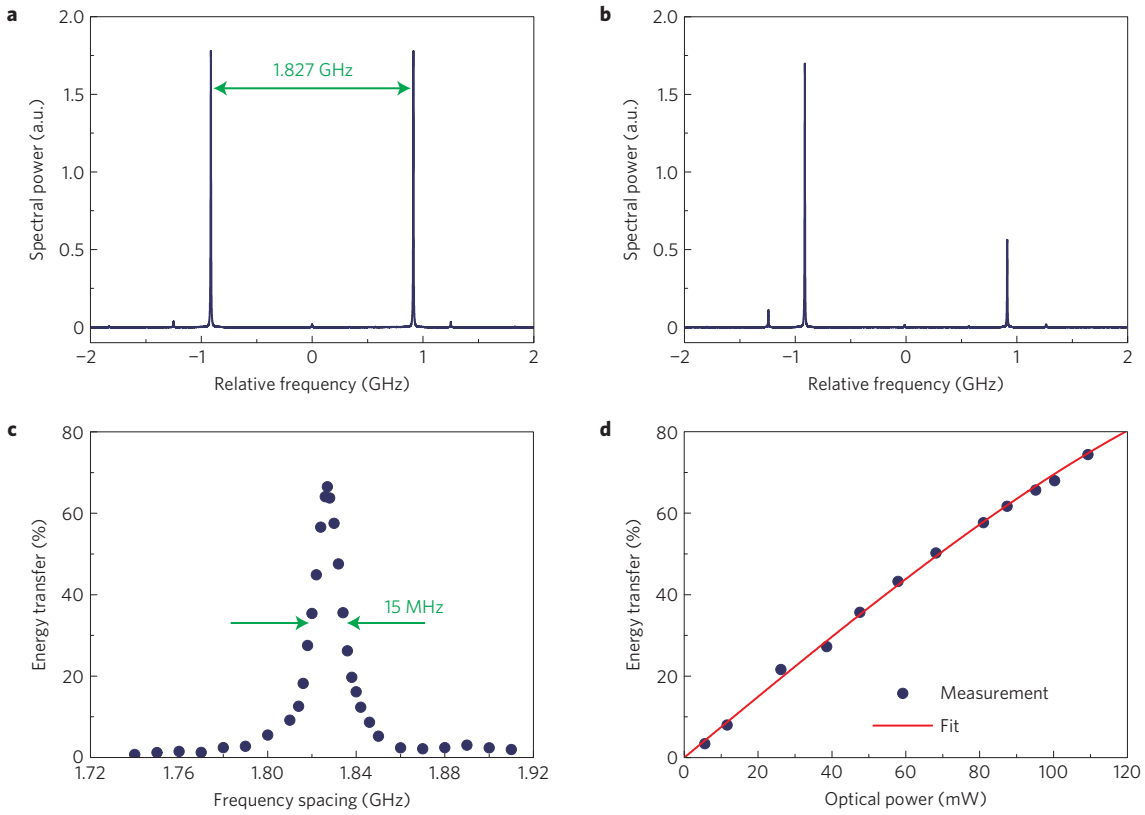

Figure 4 | Characteristics of Stokes process resulting from stimulated forward scattering. a, Spectrum of the dual-frequency light source. **b**, Energy transfer to the lower-frequency component after propagation through the PCF. Zero relative frequency corresponds to the frequency of the external cavity diode laser. The small peak at −1.26 GHz corresponds to the anti-Stokes component of which the actual relative frequency is 2.74 GHz. **c**, Dependence of the Stokes energy transfer on the frequency spacing of the light source for 90 mW pump power. **d**, Dependence of the Stokes energy transfer on the incident power of dual-frequency light at resonance (1.83 GHz frequency spacing). The fit was carried out using equation (6).

variation of the R_{01} acoustic mode. The brackets $\langle\ \rangle$ represent the overlap integral over the fibre cross-section and $\nabla_{\perp}^2$ is the Laplacian acting on the transverse coordinates. According to equation (2), the low-frequency component is amplified and the high-frequency component is attenuated during propagation in the PCF. Furthermore, this process shows a resonant behaviour with a Lorentzian gain spectrum. These points agree well with the experimental results in Fig. 4. We note that equation (2) is valid when the higher-order side bands are not significantly created. The general case of multiple side-band generation will be analysed later.

We can estimate the gain factor g_0 by approximating the PCF core (surrounded by an array of air channels) as a cylindrical silica rod surrounded by air (see Supplementary Section S2). Using bulk longitudinal and shear velocities of 5,996 and 3,740 m s^{-1}, the measured acoustic resonant frequency (1.83 GHz) corresponds to a silica rod of radius $a = 1.04\,\mu$m (ref. 22). Next we can obtain analytically the normalized optical field distribution E_0 (ref. 23) and the normalized density variation distribution ρ_{01} in the rod[24], from which Q_0 and Q_1 can be numerically calculated. Using $\gamma_e = 1.17$, $n_{eff} = 1.4$ and $\rho_0 = 2.20 \times 10^3$ kg m^{-3} for silica[24,25], and the experimental values $\omega_1 = 2\pi \times 194$ THz, $\Omega_a = 2\pi \times 1.83$ GHz and $\Gamma_B = 2\pi \times 15$ MHz, we estimate $g_0 \sim 3$ m^{-1} W^{-1}. This is larger by a factor of 2 than the experimentally determined gain (1.5 m^{-1} W^{-1}), which we attribute to the larger acoustic and optical mode areas in the actual PCF core compared with those in a silica strand in vacuum. This will reduce the value of the overlap integrals in the expression for g_0 in equation (2).

It is instructive to estimate the gain factor for a conventional single-mode fibre (Corning SMF-28, core diameter: 8.2 μm, refractive index difference: 0.36%, cladding diameter: 125 μm) for comparison (see Supplementary Section S2). In a small-core PCF, the R_{01}-like acoustic mode interacts most efficiently with the fundamental optical mode, whereas in SMF-28 it is the R_{06} acoustic mode that yields the highest gain factor. This is because, although in SMF-28 the acoustic energy fills the whole cladding, the R_{06} mode has the largest acousto-optic overlap with the fundamental optical mode around the core region (see Supplementary Fig. S3a). The gain factor for the R_{06} mode is estimated to be only $g_0 \sim 8 \times 10^{-3}$ m^{-1} W^{-1}, using $n_{eff} = 1.45$, $\Omega_a = 2\pi \times 275$ MHz and a mechanical quality factor of 105 (ref. 7). This is 200 times smaller than the measured gain factor in the PCF (1.5 m^{-1} W^{-1}), mainly as a result of smaller acousto-optic overlap (the acoustic mode occupies the entire fibre cross-section) and lower optical intensity in the larger core.

When the power of the dual-frequency pump is further increased, multiple higher-order Stokes and anti-Stokes components appear (Fig. 5). For input power 188 mW, the higher-frequency component is completely transferred to other frequencies (Fig. 5a), whereas at 324 mW it recovers (Fig. 5b). The number of side bands grows monotonically with increasing pump power, the amplitude of each oscillating in a complex manner. At the maximum input power available in the set-up (471 mW), 12 new frequency components were generated, spanning the range −12 to +12 GHz (Fig. 5c).

To analyse the generation of multiple side bands, the model is extended to include all of the higher-order Stokes and anti-Stokes components at equidistant frequencies $\omega_n = \omega_0 + n\Omega$ (n: integer):

$$E(r,z,t) = E_0(r)\sum_n a_n(z,t)\exp[i(\beta_n z - \omega_n t)] + \text{c.c.} \qquad (3)$$

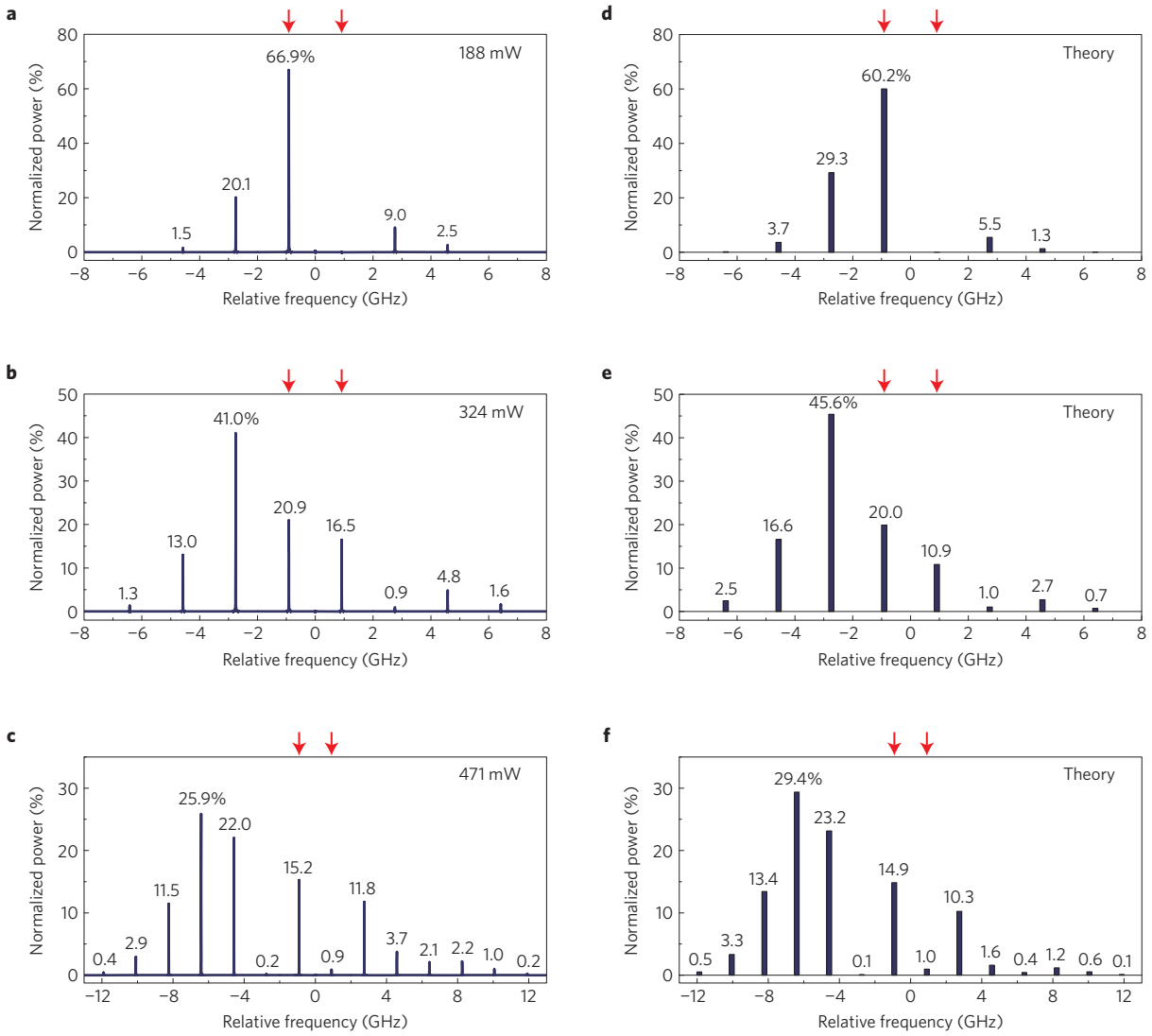

Figure 5 | Optical spectra of the transmitted light showing generation of multiple Stokes and anti-Stokes components. For clarity, the spectra are unfolded considering the 4 GHz FSR of the Fabry–Perot spectrum analyser. The power in each side band is expressed as a percentage of the total pump power. Red downward-pointing arrows indicate the two components of the dual-frequency pump light. **a**, Coupled optical power 188 mW; note that the higher-frequency component (0.9135 GHz) of the dual-frequency light is totally transferred to the other components. **b**, Coupled power 324 mW. **c**, Coupled power 471 mW, which is the maximum power available in the experiment. **d**–**f**, The theoretically modelled optical spectra corresponding to **a**–**c**, respectively.

In the steady-state regime, this leads to an infinite set of coupled differential equations (full details are available in Supplementary Section S2):

$$b(z) = \varepsilon_0 \gamma_e Q_1 \frac{\sum_n a_{n-1}^* a_n}{\Omega^2 - \Omega_a^2 + i\,\Omega\Gamma_B} \tag{4}$$

$$\frac{\partial a_n}{\partial z} = \frac{i\omega_1 \gamma_e Q_0}{2n_{\mathrm{eff}} c \rho_0} (a_{n-1} b + a_{n+1} b^*) \tag{5}$$

where ε_0 is the electric permittivity in vacuum. As the spectral width of the frequency comb generated in the experiment is much smaller than the carrier frequency of the optical waves, we approximate $\omega_n \approx \omega_1$ and $\beta_n \approx \beta_1$ for all values of n. Combining equations (4) and (5) yields after some manipulation $\partial b(z)/\partial z = 0$, which means that $b(z)$ has a constant value throughout the PCF, depending on the initial values of $a_n(z=0)$. In the case of a dual-frequency pump with exact phase-matching ($\Omega = \Omega_a$), the solutions of equations (4) and (5) are:

$$b(z) = b(0) = \frac{i\gamma_e |Q_1|}{2n_{\mathrm{eff}} c \Omega_a \Gamma_B} \sqrt{P_1(0) P_2(0)}\, e^{i\varphi_0}$$

$$a_n(\xi) = a_1(0)\, e^{i(n-1)(\varphi_0 - \pi)} J_{n-1}(\xi) + a_2(0)\, e^{i(n-2)(\varphi_0 - \pi)} J_{n-2}(\xi) \tag{6}$$

where φ_0 is the phase difference of the two incident fields at the input port, $\xi \equiv g_0 z \sqrt{P_1(0) P_2(0)}$ is defined as the normalized propagation length and J_n is an nth-order Bessel function of the first kind.

The gain coefficient g_0 (previously estimated to be $1.5\,\mathrm{m^{-1}\,W^{-1}}$) yields normalized lengths of $\xi = 1.4$, 2.4 and 3.5 for the three incident optical powers in Fig. 5a–c. Figure 5d–f shows the theoretically modelled spectra that fit best to the experimental data in Fig. 5a–c. They were obtained by using equation (6) with $\xi = 1.44$, 2.25 and 4.4, respectively, and show good agreement with the corresponding experimental values.

Equation (6) indicates that the frequency comb is coherent; that is, the phases of all its components are locked to the dual-frequency pump. The total electric field in equation (3) takes the form:

$$E(r,z,t) = E_0(r)\{a_1(0)e^{i(\beta_1 z-\omega_1 t)} + a_2(0)e^{i(\beta_2 z-\omega_2 t)}\} \times e^{-i\xi\sin[(q_a z-\Omega_a t)+\varphi_0]} + \text{c.c.}$$

showing that both components of the dual-frequency pump experience the same phase modulation, with a frequency chirp that oscillates (under the intensity envelope) at the acoustic resonant frequency. If the side-band phases are suitably adjusted by introducing an appropriate frequency-dependent phase delay, this will produce a train of optical pulses of duration $\sim 2\pi/N\Omega_a$ (N is the total number of side bands) at a repetition frequency of $\Omega_a/2\pi$.

Finally, it is quite possible to design a structure where the acoustic resonance is confined by a phononic bandgap in the cladding[4,5], thus strongly suppressing leakage of energy into the cladding. According to our discussion above, this would result in a 20 times smaller Brillouin linewidth ($\tau_{\text{leakage}} \to \infty$ in equation (1)), 20 times higher gain and much stronger side-band generation—provided of course that fibre non-uniformities can be reduced to a minimum.

Received 2 September 2008; accepted 6 February 2009; published online 22 March 2009

References

1. Gorishnyy, T., Jang, J. H., Koh, C. & Thomas, E. L. Direct observation of a hypersonic band gap in two-dimensional single crystalline phononic structures. *Appl. Phys. Lett.* **91**, 121915 (2007).
2. Trigo, M., Bruchhausen, A., Fainstein, A., Jusserand, B. & Thierry-Mieg, V. Confinement of acoustical vibrations in a semiconductor planar phonon cavity. *Phys. Rev. Lett.* **89**, 227402 (2002).
3. Arcizet, O., Cohadon, P.-F., Briant, T., Pinard, M. & Heidmann, A. Radiation-pressure cooling and optomechanical instability of a micromirror. *Nature* **444**, 71–74 (2006).
4. Dainese, P. *et al.* Raman-like light scattering from acoustic phonons in photonic crystal fiber. *Opt. Express* **14**, 4141–4150 (2006).
5. Beugnot, J.-C., Sylvestre, T., Maillotte, H., Mélin, G. & Laude, V. Guided acoustic wave Brillouin scattering in photonic crystal fibers. *Opt. Lett.* **32**, 17–19 (2007).
6. Wiederhecker, G. S., Brenn, A., Fragnito, H. L. & Russell, P. St.J. Coherent control of ultrahigh-frequency acoustic resonances in photonic crystal fibers. *Phys. Rev. Lett.* **100**, 203903 (2008).
7. Shelby, R. M., Levenson, M. D. & Bayer, P. W. Guided acoustic-wave Brillouin scattering. *Phys. Rev. B* **31**, 5244–5252 (1985).
8. Elser, D. *et al.* Reduction of guided acoustic wave Brillouin scattering in photonic crystal fibers. *Phys. Rev. Lett.* **97**, 133901 (2006).
9. Kim, S. *et al.* High-harmonic generation by resonant plasmon field enhancement. *Nature* **453**, 757–760 (2008).
10. Fukuba, S., Tsuboi, K., Abe, S. & Kajikawa, K. Nonlinear optical detection of proteins based on localized surface plasmons in surface immobilized gold nanospheres. *Langmuir* **24**, 8367–8372 (2008).
11. Chang, D. E., Sørensen, A. S., Demler, E. A. & Lukin, M. D. A single-photon transistor using nanoscale surface plasmons. *Nature Phys.* **3**, 807–812 (2007).
12. Spillane, S. M., Kippenberg, T. J. & Vahala, K. J. Ultralow-threshold Raman laser using a spherical dielectric microcavity. *Nature* **415**, 621–623 (2002).
13. Del'Haye, P. *et al.* Optical frequency comb generation from a monolithic microresonator. *Nature* **450**, 1214–1217 (2007).
14. Sensarn, S., Goda, S. N., Yin, G. Y. & Harris, S. E. Molecular modulation in a hollow fiber. *Opt. Lett.* **31**, 2836–2838 (2006).
15. Niklès, M., Thévenaz, L. & Robert, P. A. Brillouin gain spectrum characterization in single-mode optical fibers. *J. Lightwave Tech.* **15**, 1842–1851 (1997).
16. Dainese, P. *et al.* Stimulated Brillouin scattering from multi-GHz-guided acoustic phonons in nanostructured photonic crystal fibres. *Nature Phys.* **2**, 388–392 (2006).
17. McElhenny, J. E., Pattnaik, R. K., Toulouse, J., Saitoh, K. & Koshiba, M. Unique characteristic features of stimulated Brillouin scattering in small-core photonic crystal fibers. *J. Opt. Soc. Am. B* **25**, 582–593 (2008).
18. Kulcsar, G., Jaouën, Y., Canat, G., Olmedo, E. & Debarge, G. Multiple-stokes stimulated Brillouin scattering generation in pulsed high-power double-cladding Er^{3+}–Yb^{3+} codoped fiber amplifier. *IEEE Photon. Tech. Lett.* **15**, 801–803 (2003).
19. Ogusu, K. Interplay between cascaded stimulated Brillouin scattering and four-wave mixing in a fiber Fabry–Perot resonator. *J. Opt. Soc. Am. B* **20**, 685–694 (2003).
20. Biryukov, A. S., Sukharev, M. E. & Dianov, E. M. Excitation of sound waves upon propagation of laser pulses in optical fibres. *Quantum Electron.* **32**, 765–775 (2002).
21. Dianov, E. M., Luchnikov, A. V., Pilipetskii, A. N. & Starodumov, A. N. Electrostriction mechanism of soliton interaction in optical fibers. *Opt. Lett.* **15**, 314–316 (1990).
22. Thurston, R. N. Elastic waves in rods and clad rods. *J. Acoust. Soc. Am.* **64**, 1–37 (1978).
23. Okoshi, T. *Optical Fibers* (Academic, 1982).
24. Peral, E. & Yariv, A. Degradation of modulation and noise characteristics of semiconductor lasers after propagation in optical fiber due to a phase shift induced by stimulated Brillouin scattering. *IEEE J. Quantum Electron.* **35**, 1185–1195 (1999).
25. Boyd, R. W. *Nonlinear Optics* (Academic, 2008).

Additional information

Supplementary Information accompanies this paper on www.nature.com/naturephysics. Reprints and permissions information is available online at http://npg.nature.com/reprintsandpermissions. Correspondence and requests for materials should be addressed to P.St.J.R.